Photocatalysis

DOI: 10.1002/anie.201408868

Nanocomposites of Tantalum-Based Pyrochlore and Indium Hydroxide Showing High and Stable Photocatalytic Activities for Overall Water Splitting and Carbon Dioxide Reduction**

*Meng-Chun Hsieh, Guan-Chang Wu, Wei-Guang Liu, William A. Goddard III, and Chia-Min Yang**

Abstract: *Nanocomposites of tantalum-based pyrochlore nanoparticles and indium hydroxide were prepared by a hydrothermal process for UV-driven photocatalytic reactions including overall water splitting, hydrogen production from photoreforming of methanol, and CO_2 reduction with water to produce CO. The best catalyst was more than 20 times more active than sodium tantalate in overall water splitting and 3 times more active than Degussa P25 TiO_2 in CO_2 reduction. Moreover, the catalyst was very stable while generating stoichiometric products of H_2 (or CO) and O_2 throughout long-term photocatalytic reactions. After the removal of $In(OH)_3$, the pyrochlore nanoparticles remained highly active for H_2 production from pure water and aqueous methanol solution. Both experimental studies and density functional theory calculations suggest that the pyrochlore nanoparticles catalyzed the water reduction to produce H_2, whereas $In(OH)_3$ was the major active component for water oxidation to produce O_2.*

Direct photocatalytic conversion of water and CO_2 into solar fuels is an attractive prospect, serving to provide an alternative energy source on a renewable basis.[1] A variety of photocatalysts have been examined for the two reactions. For the overall water splitting to produce H_2 and O_2, TiO_2 and other perovskite materials[2] are among the most widely studied photocatalysts. In most cases, cocatalysts composed of noble metals[3] with proper Fermi level or metal oxides[3] with suitable band positions are necessary to suppress charge recombination and enhance photocatalytic activity. The oxidation of water is more difficult to catalyze, and a hole scavenger such as methanol or acetone is often added (that is, photo-reforming instead of water splitting) for H_2 production.[1b,4] As compared to water splitting, photocatalytic CO_2 reduction with water as a reductant is even more challenging.[4,5] The active catalysts for water splitting would be expected to be also active for CO_2 reduction because of the high reduction potential of the photoexcited electrons, but most of them reduce water instead of CO_2 in the mixture of CO_2 and water.[6] This may be because CO_2 reduction involves multiple electrons and steps, making it kinetically slower.[5a] To date, very few catalysts are capable of catalyzing both water splitting and CO_2 reduction with Pt/TiO_2[6a] among the best. Several photocatalytic systems have also been reported for CO_2 reduction, such as Cu/TiO_2,[7] $Pt/CaFe_2O_4$,[8] C and Fe co-doped $LaCoO_3$,[9] $BiVO_4$,[10] $NiO/InTaO_4$,[11] $ZnGa_2O_4$,[12] and $Pt/RuO_2/Zn_2GeO_4$,[13] but conversion remains low and the stability is often poor. Moreover, the loading processes of effective cocatalysts are often complicated with problems of reproducibility.[1b,14]

Herein we report a novel photocatalyst comprising tantalum-based pyrochlore (TP) nanoparticles. Cubic pyrochlore is a metastable crystal structure similar to defective perovskite structure.[15] Owing to the flexibility of the structure, pyrochlore compounds form over a huge compositional range with a variety of properties and applications.[16] However, only a rather limited number of pyrochlore compounds have been reported to be active for photocatalytic applications, and these are mainly for photodecomposition of organic compounds and photoreforming of oxygenates to produce H_2.[17] Pyrochlore-based photocatalysts are generally less active than Ti-, Nb-, and Ta-based perovskites for water splitting,[18] and none of them shows photocatalytic activity for CO_2 reduction.

Recently, we discovered a hydrothermal process to prepare composites of TP nanoparticles and indium hydroxide ($In(OH)_3$), and pure TP nanoparticles after acid dissolution of $In(OH)_3$. We found that TP alone could efficiently catalyze methanol photoreforming to produce H_2. More surprisingly, the TP/$In(OH)_3$ nanocomposite synthesized with optimum conditions showed high and stable photocatalytic activities for both overall water splitting and CO_2 reduction with water and generated stoichiometric amounts of the corresponding products. We carried out calculations to estimate relative band structures of TP and $In(OH)_3$ that suggest redox sites in the nanocomposites. These results show

[*] M.-C. Hsieh, G.-C. Wu, Prof. Dr. C.-M. Yang
Department of Chemistry, National Tsing Hua University
Hsinchu 30013 (Taiwan)
E-mail: cmyang@mx.nthu.edu.tw
Dr. W.-G. Liu, Prof. W. A. Goddard III
Materials and Process Simulation Center
California Institute of Technology, Pasadena, CA 91125 (USA)
Prof. Dr. C.-M. Yang
Frontier Research Center on Fundamental and Applied Sciences of Matters, National Tsing Hua University
Hsinchu 30013 (Taiwan)

[**] We thank the Ministry of Science and Technology for the financial support under the contract nos. MOST 101-2628-M-007-001-MY2 and MOST 103-3113-P-008-001-.

Supporting information for this article (including details of materials synthesis, characterization, photocatalytic reaction, and DFT calculations) is available on the WWW under http://dx.doi.org/10.1002/anie.201408868.

immense promise for a new type of photocatalysts for energy and environmental-related reactions.

The materials were prepared under alkaline hydrothermal conditions at 170–220 °C using $K_8[Ta_6O_{19}]\cdot 14H_2O$[19] and indium chloride as metal precursors (see the Experimental Section in the Supporting Information). The materials (designated as TIM-*x*, where *x* denotes the hydrothermal temperature) were composed of the pyrochlore phase (ICSD-24225) and the cubic $In(OH)_3$ (ICSD-35636), as indicated by their X-ray diffraction (XRD) patterns (Figure 1; Supporting Information, Figure S1). Scanning electron microscopy

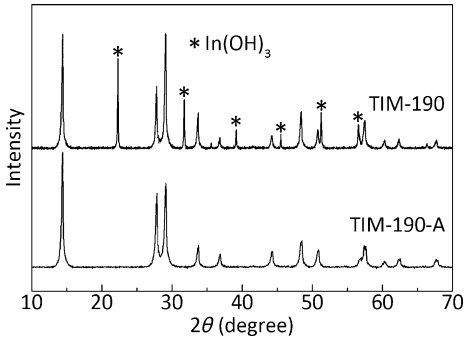

Figure 1. XRD patterns of TIM-190 and TIM-190-A.

(SEM) showed that these samples consist mainly of 30–40 nm octahedral-shaped particles coexisting with a few large (400–700 nm) particles (see the Supporting Information, Figure S2 for the image of TIM-190). The large particles were $In(OH)_3$, as suggested by energy-dispersive X-ray spectrometry (EDX) indicating much higher amounts of indium in these particles (Supporting Information, Figure S2). The octahedral-shaped nanoparticles were further characterized by transmission electron microscopy (TEM), with a typical image of TIM-190 in Figure 2a. There is clearly a lattice fringe corresponding to the (111) planes of pyrochlore throughout each nanoparticle, indicating the single-crystalline nature of these nanoparticles. Moreover, tiny and highly dispersed clusters were observed on the pyrochlore nanoparticles. The clusters were identified as $In(OH)_3$ because treating the samples with aqueous solution of hydrochloric acid completely removed them together with the large $In(OH)_3$ particles, as shown by XRD and TEM analyses of the acid-treated samples, denoted as TIM-x-A (Figure 1, 2b; Supporting Information, Figure S1). The TP nanoparticles retained the octahedral shape and high crystallinity after the acid treatment but, noticeably, they appeared with non-uniform contrast in TEM images, implying the presence of extensive defects in these nanoparticles.

We then determined the formulas of TIM-*x* and TIM-*x*-A samples. Inductively coupled plasma-mass spectroscopy (ICP-MS) showed that TIM-190 and TIM-190-A had K/In/Ta ratios of 0.66:0.46:1 and 0.14:0.03:1, respectively. We expect that the additional amount of indium in TIM-190 (in comparison to that in TIM-190-A) is in the form of $In(OH)_3$. Furthermore, the much higher K/Ta ratio for TIM-190 suggests that extensive potassium/proton exchange took place during the

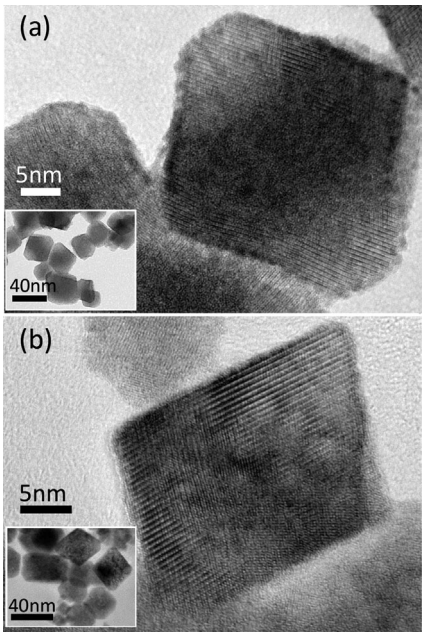

Figure 2. TEM images of a) TIM-190 and b) TIM-190-A.

acid treatment. The presence of exchanged protons was confirmed by ^1H NMR (Supporting Information, Figure S3). For the metal cations of K^{1+}, In^{3+}, and Ta^{5+}, the balanced formulas of pure-phase TIM-*x*-A had tantalum-to-oxygen ratios of 2:5.23–5.29 (Supporting Information, Table S1). This indicates that the TP nanoparticles have the defect pyrochlore ($A_2B_2O_6$) structure rather than an ideal pyrochlore ($A_2B_2O_7$) structure.[20] Furthermore, the relative amount of crystallization water was quantified by thermal gravimetric analysis–mass spectroscopy (TGA-MS; Supporting Information, Figure S4).[21] Based on all these results, we determined complete formulas for all samples (Supporting Information, Table S1). It seems that an increase of hydrothermal temperature results in defect TP materials with more indium (or higher In/Ta) but less potassium (or lower K/Ta). For TIM-190-A and TIM-190, the deduced formulas are $H_{1.55}K_{0.27}In_{0.06}Ta_2O_6\cdot 0.8H_2O$ and $H_{0.50}K_{1.32}In_{0.06}Ta_2O_6\cdot 2.2H_2O/0.86\,In(OH)_3$, respectively.

The TIM-*x* and TIM-*x*-A samples absorbed UV light, with the main absorption edges at around 270 nm (corresponding to band gaps of 4.6–4.8 eV; Supporting Information, Figure S5), and we studied their activities for UV-driven photoreforming of methanol and overall water splitting. Figure 3a compares the average H_2 evolution rates from 10 vol% methanol aqueous solution by TIM-*x*, TIM-*x*-A, and a benchmark photocatalyst sodium tantalate ($NaTaO_3$).[14a] All of the samples outperformed $NaTaO_3$, while the $In(OH)_3$-free TIM-x-A was more active than TIM-x. TIM-190 A was the best photocatalyst exhibiting the very high H_2 evolution rate of 5.82 mmol $g^{-1}h^{-1}$. Obviously, the defect TP nanoparticles must be the major active component for H_2 production even though $In(OH)_3$ also absorbs UV light (Supporting Information, Figure S5). We further examined the activities for overall water splitting. Again, we found that all samples (except TIM-170) were more active than the benchmark catalyst while TIM-190 and TIM-190-A were the most active

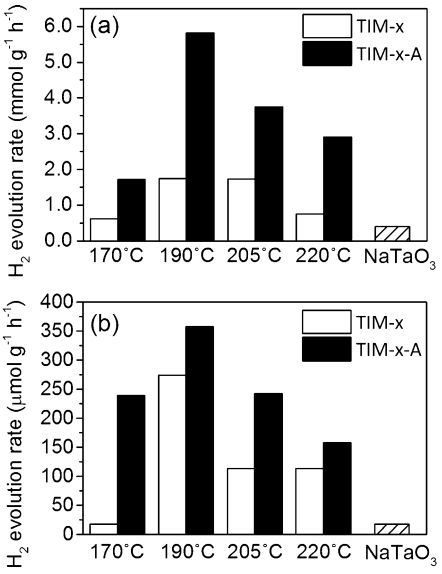

Figure 3. Comparison of photocatalytic H_2 evolution rates from a) 10 vol% methanol and b) pure water on TIM-*x*, TIM-*x*-A, and $NaTaO_3$ at 25 °C.

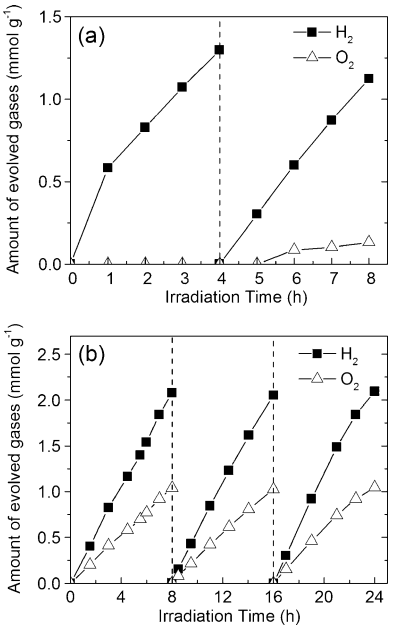

Figure 4. Time courses of photocatalytic water splitting on a) TIM-190-A and b) TIM-190. The reactions were continued for 8 h (a) or 24 h (b), with argon purge (-----) every 4 h (a) or 8 h (b).

among the same type of samples (Figure 3b). Since the TP nanoparticles in all samples had similar particle size, crystallinity, and band gap, the observed volcano-shaped relationship between H_2 evolution rate and hydrothermal temperature for the two reactions must be associated with the composition variations, which is likely to be the relative amount of OH^- groups (that is, the stoichiometry of H in the formulas; Supporting Information, Table S1) which also peaks at 190 °C. Remarkably, the H_2 evolution rate (357.7 μmol g^{-1} h^{-1}) of TIM-190-A is more than twenty times higher than that (17.0 μmol g^{-1} h^{-1}) of $NaTaO_3$. For comparison, the evolution rates for Degussa P25 TiO_2, Ta_2O_5, and NiO-loaded (3 wt%) $SrTiO_3$[2g] measured under identical conditions were 0.1, 1.8, and 24.7 μmol g^{-1} h^{-1}, respectively. With the benchmark photocatalysts as references,[2,3,4,14a] the activity of TIM-190 A is comparable to those of highly active metal-doped and cocatalyst-loaded Ta-based pervoskites[22] except the La-doped NiO-loaded $NaTaO_3$.[14a] However, the NiO-loaded photocatalysts suffer from severe deactivation owing to the elution of nickel species[14a] and they did not show stable activities in pure water. For TIM-190-A, the apparent quantum yield obtained with 232 nm radiation (full width half-maximum of the intensity = 10 nm) for 2 h was 0.55%.

We then examined the time courses of H_2 and O_2 evolution from water splitting on TIM-190-A and TIM-190, with typical results shown in Figure 4. Despite of showing high H_2 evolution rate, TIM-190-A produced very little O_2, and no O_2 was detected within the first six hours. The formation of O_2 is much more challenging because it involves four-electron oxidation of water,[22b] whereas it seems that most holes photogenerated in the TP nanoparticles are consumed to form other species.[22b] Indeed, a significant amount of H_2O_2 was detected in the TIM-190-A-containing solution after 8 h irradiation by the redox titration with $KMnO_4$.[23] In contrast, TIM-190 showed stable and stoichiometric evolution of H_2 and O_2, which was evident from the start of the reaction. No noticeable degradation of activity was observed in repeated runs for 24 h. In comparison to the pure-phase TIM-190-A, the excellent photocatalytic performance of TIM-190 for water splitting is associated mainly with the presence of $In(OH)_3$ nanoparticles that may utilize the photogenerated holes to oxidize water and produce O_2 as efficiently as the reduction of water to produce H_2.

With these encouraging results for water splitting, we further investigated the photocatalytic performance in gas-phase CO_2 reduction with saturated water vapor at 25 °C with $NaTaO_3$ and Degussa P25 TiO_2 as benchmark photocatalysts. We found that TIM-190 again exhibited the highest CO evolution rate of 14.2 μmol g^{-1} h^{-1} (Figure 4a), while most samples of TIM-*x* and TIM-*x*-A showed very low activities. More importantly, the TIM-190 catalyst produced stoichiometric amounts of CO and O_2 with 2:1 ratio from the start of UV irradiation (Figure 4b), indicating that it catalyzed the reduction of CO_2 with water as a reductant according to the following equations:

$$CO_2 + 2H^+ + 2e^- \rightarrow CO + H_2O \quad (1)$$

$$H_2O \rightarrow {}^1/_2 O_2 + 2H^+ + 2e^- \quad (2)$$

The fact that no H_2 was detected further suggests that the TIM-190 catalyst selectively reduces CO_2 instead of water. Again, the presence of $In(OH)_3$ in TIM-190 appeared to be crucial for water oxidation to produce O_2. To the best of our knowledge, there are very few Ta-based photocatalysts reported for CO_2 reduction with water and none of them could give stoichiometric products of the redox reactions.[24]

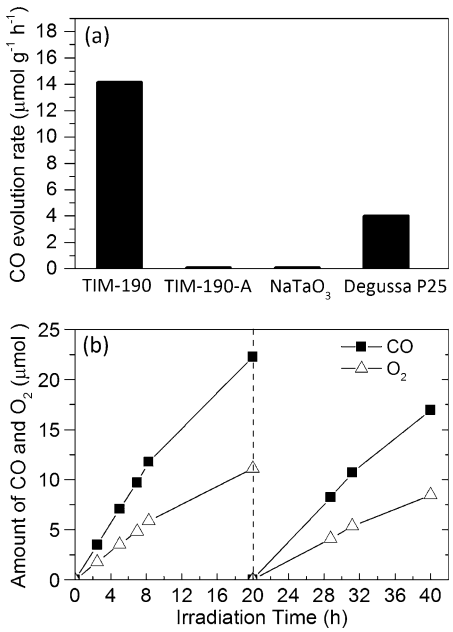

Figure 5. a) Comparison of evolution rates of CO from photocatalytic CO_2 reduction with water on selected samples. b) Time course of photocatalytic CO_2 reduction with water on TIM-190. The reaction was continued for 40 h with CO_2 purge (-----) at 20 h.

In contrast, the activity of TIM-190 is three times higher than Degussa P25 (Figure 5a) and is higher or comparable to most TiO_2-based materials.[25] For the metal-loaded TiO_2 materials[7a] and defective TiO_2[26] that were reported to be highly active for the reaction, catalytic stability is often a problem. An example is the reaction catalyzed by Pt-loaded TiO_2 to produce CO and CH_4,[6a] where a circa 80% decrease in the CH_4 evolution rate was observed within the first six hours of reaction. Interestingly, TIM-190 exhibited rather stable activity for the first eight hours and decreased only slightly in the following twelve hours (Figure 5b). This catalyst was reused after CO_2 purging and still showed stoichiometric gas production and CO evolution rate of 8.4 $\mu mol\,g^{-1}\,h^{-1}$.

These photocatalytic studies suggest strongly that $In(OH)_3$ plays the crucial role in the nanocomposite TIM-190 in water oxidation. It has been shown that the Pt-loaded mesoporous $In(OH)_3$ is active for CO_2 reduction, but no O_2 evolution was observed.[27] In our study, the observed effective water oxidation is likely associated with enhanced charge separation caused by heterojunction interfaces between $In(OH)_3$ and the defect TP.

To clarify these issues, we performed density functional theory (DFT) calculations aimed at understanding the band alignment between these two materials. We constructed a two-layer (100) slabs terminated by OH to evaluate the absolute band positions of $In(OH)_3$ and the defect TP (see Part IV in the Supporting Information for details in calculation). We used the B3PW91 DFT functional, as we find that it accurately reproduce the bandgap of many semiconductors to about 0.1 eV.[28] For the $In(OH)_3$ slab, this leads to the top of the valance band (VB) at −7.07 V and the bottom level of the conduction band (CB) at −0.97 V (relative to vacuum level; Supporting Information, Figure S7a). For the TP slab, the corresponding levels of the VB and CB are −7.61 V and −2.28 V, respectively (Supporting Information, Figure S7b). We also tested other less accurate functionals, such as B3LYP, PBE and PBE0, and found that the band positions range over the range of about 1.5 V (Supporting Information, Table S2). However in all of the cases we find that the VB and CB of $In(OH)_3$ are always higher than those of TP. Thus based on these DFT results, we conclude that the heterojunction between $In(OH)_3$ and TP is as shown in Scheme 1, the electrons generated upon UV irradiation in the CB of TP nanoparticles reduce water or CO_2 to produce H_2 or CO, whereas the holes are transferred to the VB of $In(OH)_3$ for water oxidation to produce O_2.

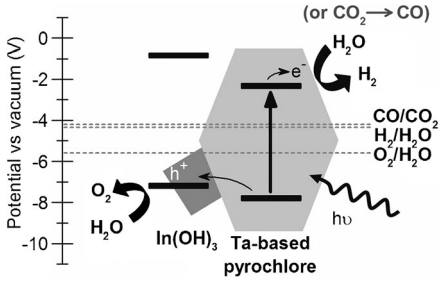

Scheme 1. Diagram of photocatalytic overall water splitting and CO_2 reduction with water on TIM-190 containing nanocomposites of $In(OH)_3$ and defect TP nanoparticles.

In summary, we successfully prepared nanocomposites of tantalum-based pyrochlore nanoparticles and $In(OH)_3$ for photocatalytic water splitting and CO_2 reduction with water. We find that the defect pyrochlore nanoparticles catalyze the water reduction to produce hydrogen, whereas $In(OH)_3$ is the major active component for water oxidation. With optimum hydrothermal synthesis conditions, the nanocomposite shows superior and stable catalytic performance while generating stoichiometric products. After the removal of $In(OH)_3$ from the nanocomposites, the pure-phase pyrochlore nanoparticles remain highly active for hydrogen production from pure water and methanol aqueous solution. We envision that this discovery will lead to further development of highly efficient photocatalysts for solar fuels production and other reactions.

Received: September 6, 2014
Revised: October 20, 2014
Published online: November 10, 2014

Keywords: CO_2 reduction · indium hydroxide · photocatalysis · tantalum-based pyrochlore · water splitting

[1] a) G. Centi, S. Perathoner, *ChemSusChem* **2010**, *3*, 195–208; b) X. Chen, S. Shen, L. Guo, S. S. Mao, *Chem. Rev.* **2010**, *110*, 6503–6570.

[2] a) H. Kato, K. Asakura, A. Kudo, *J. Am. Chem. Soc.* **2003**, *125*, 3082–3089; b) H. Kato, A. Kudo, *J. Phys. Chem. B* **2001**, *105*, 4285–4292; c) T. Ishihara, H. Nishiguchi, K. Fukamachi, Y. Takita, *J. Phys. Chem. B* **1999**, *103*, 1–3; d) L. Chen, S. Zhang, L.

Wang, D. Xue, S. Yin, *J. Cryst. Growth* **2009**, *311*, 735 – 737; e) Y. Noda, B. Lee, K. Domen, J. N. Kondo, *Chem. Mater.* **2008**, *20*, 5361 – 5367; f) H. J. Zhang, G. Chen, Z. H. Li, *Appl. Surf. Sci.* **2007**, *253*, 8345 – 8351; g) T. K. Townsend, N. D. Browning, F. E. Osterloh, *ACS Nano* **2012**, *6*, 7420 – 7426.

[3] a) F. E. Osterloh, *Chem. Soc. Rev.* **2013**, *42*, 2294 – 2320; b) J. Yang, D. Wang, H. Han, C. Li, *Acc. Chem. Res.* **2013**, *46*, 1900 – 1909.

[4] A. Kudo, Y. Miseki, *Chem. Soc. Rev.* **2009**, *38*, 253 – 278.

[5] a) S. Navalon, A. Dhakshinamoorthy, M. Alvaro, H. Garcia, *ChemSusChem* **2013**, *6*, 562 – 577; b) Y. Izumi, *Coord. Chem. Rev.* **2013**, *257*, 171 – 186.

[6] a) W. N. Wang, W. J. An, B. Ramalingam, S. Mukherjee, D. M. Niedzwiedzki, S. Gangopadhyay, P. Biswas, *J. Am. Chem. Soc.* **2012**, *134*, 11276 – 11281; b) A. Dhakshinamoorthy, S. Navalon, A. Corma, H. Garcia, *Energy Environ. Sci.* **2012**, *5*, 9217 – 9233; c) S. N. Habisreutinger, L. Schmidt-Mende, J. K. Stolarczyk, *Angew. Chem. Int. Ed.* **2013**, *52*, 7372 – 7408; *Angew. Chem.* **2013**, *125*, 7516 – 7557; d) K. Iizuka, T. Wato, Y. Miseki, K. Saito, A. Kudo, *J. Am. Chem. Soc.* **2011**, *133*, 20863 – 20868; e) X.-J. Lv, W.-F. Fu, C.-Y. Hu, Y. Chen, W.-B. Zhou, *RSC Adv.* **2013**, *3*, 1753 – 1753.

[7] a) L. Liu, F. Gao, H. Zhao, Y. Li, *Appl. Catal. B* **2013**, *134 – 135*, 349 – 358; b) K. Adachi, K. Ohta, T. Mizuno, *Sol. Energy* **1994**, *53*, 187 – 190; c) O. K. Varghese, M. Paulose, T. J. LaTempa, C. A. Grimes, *Nano Lett.* **2009**, *9*, 731 – 737.

[8] a) Y. Matsumoto, *J. Solid State Chem.* **1996**, *126*, 227 – 234; b) Y. Matsumoto, M. Obata, J. Hombo, *J. Phys. Chem.* **1994**, *98*, 2950 – 2951.

[9] L. Jia, J. Li, W. Fang, *Catal. Commun.* **2009**, *11*, 87 – 90.

[10] Y. Liu, B. Huang, Y. Dai, X. Zhang, X. Qin, M. Jiang, M.-H. Whangbo, *Catal. Commun.* **2009**, *11*, 210 – 213.

[11] P.-W. Pan, Y.-W. Chen, *Catal. Commun.* **2007**, *8*, 1546 – 1549.

[12] S. C. Yan, S. X. Ouyang, J. Gao, M. Yang, J. Y. Feng, X. X. Fan, L. J. Wan, Z. S. Li, J. H. Ye, Y. Zhou, Z. G. Zou, *Angew. Chem. Int. Ed.* **2010**, *49*, 6400 – 6404; *Angew. Chem.* **2010**, *122*, 6544 – 6548.

[13] a) Q. Liu, Y. Zhou, J. Kou, X. Chen, Z. Tian, J. Gao, S. Yan, Z. Zou, *J. Am. Chem. Soc.* **2010**, *132*, 14385 – 14387; b) N. Zhang, S. Ouyang, P. Li, Y. Zhang, G. Xi, T. Kako, J. Ye, *Chem. Commun.* **2011**, *47*, 2041 – 2043.

[14] a) H. Kato, K. Asakura, A. Kudo, *J. Am. Chem. Soc.* **2003**, *125*, 3082 – 3089; b) G. W. Busser, B. Mei, A. Pougin, J. Strunk, R. Gutkowski, W. Schuhmann, M.-G. Willinger, R. Schloegl, M. Muhler, *ChemSusChem* **2014**, DOI: 10.1002/cssc.201301065; c) J. Xing, Y. H. Li, H. B. Jiang, Y. Wang, H. G. Yang, *Int. J. Hydrogen Energy* **2014**, *39*, 1237 – 1242; d) K. Maeda, A. Xiong, T. Yoshinaga, T. Ikeda, N. Sakamoto, T. Hisatomi, M. Takashima, D. Lu, M. Kanehara, T. Setoyama, T. Teranishi, K. Domen, *Angew. Chem. Int. Ed.* **2010**, *49*, 4096 – 4099; *Angew. Chem.* **2010**, *122*, 4190 – 4193.

[15] D. R. Modeshia, R. I. Walton, *Chem. Soc. Rev.* **2010**, *39*, 4303 – 4325.

[16] M. A. Subramanian, G. Aravamudan, G. V. Subba Rao, *Prog. Solid State Chem.* **1983**, *15*, 55 – 143.

[17] a) P. Kanhere, Y. Tang, J. Zheng, Z. Chen, *J. Phys. Chem. Solids* **2013**, *74*, 1708 – 1713; b) L. M. Torres-Martinez, I. Juarez-Ramirez, J. S. Ramos-Garza, F. Vazquez-Acosta, S. W. Lee, *Mater. Sci. Forum* **2010**, *658*, 491 – 494; c) S. Uma, J. Singh, V. Thakral, *Inorg. Chem.* **2009**, *48*, 11624 – 11630; d) J. Liu, J. Liu, Z. Li, *J. Solid State Chem.* **2013**, *198*, 192 – 196; e) A. Mukherji, R. Marschall, A. Tanksale, C. Sun, S. C. Smith, G. Q. Lu, L. Wang, *Adv. Funct. Mater.* **2011**, *21*, 126 – 132.

[18] a) H. Yang, X. Liu, Z. Zhou, L. Guo, *Catal. Commun.* **2013**, *31*, 71 – 75; b) C.-C. Hu, T.-F. Yeh, H. Teng, *Catal. Sci. Technol.* **2013**, *3*, 1798 – 1804.

[19] T. M. Anderson, M. A. Rodriguez, F. Bonhomme, J. N. Bixler, T. M. Alam, M. Nyman, *Dalton Trans.* **2007**, 4517 – 4522.

[20] N. Duan, Z.-R. Tian, W. S. Willis, S. L. Suib, J. M. Newsam, S. M. Levine, *Inorg. Chem.* **1998**, *37*, 4697 – 4701.

[21] G. K. L. Goh, S. M. Haile, C. G. Levi, F. F. Lange, *J. Mater. Res.* **2002**, *17*, 3168 – 3176.

[22] a) A. Iwase, H. Kato, H. Okutomi, A. Kudo, *Chem. Lett.* **2004**, *33*, 1260 – 1261; b) J. Sun, G. Chen, Y. Li, R. Jin, Q. Wang, J. Pei, *Energy Environ. Sci.* **2011**, *4*, 4052 – 4060.

[23] D. Tsukamoto, A. Shiro, Y. Shiraishi, Y. Sugano, S. Ichikawa, S. Tanaka, T. Hirai, *ACS Catal.* **2012**, *2*, 599 – 603.

[24] a) C.-W. Tsai, H. M. Chen, R.-S. Liu, K. Asakura, T.-S. Chan, *J. Phys. Chem. C* **2011**, *115*, 10180 – 10186; b) X.-J. Lv, W.-F. Fu, C.-Y. Hu, Y. Chen, W.-B. Zhou, *RSC Adv.* **2013**, *3*, 1753 – 1757.

[25] S. N. Habisreutinger, L. Schmidt-Mende, J. K. Stolarczyk, *Angew. Chem. Int. Ed.* **2013**, *52*, 7372 – 7408; *Angew. Chem.* **2013**, *125*, 7516 – 7557.

[26] L. Liu, H. Zhao, J. M. Andino, Y. Li, *ACS Catal.* **2012**, *2*, 1817 – 1828.

[27] J. Guo, S. Ouyang, T. Kako, J. Ye, *Appl. Surf. Sci.* **2013**, *280*, 418 – 423.

[28] H. Xiao, J. Tahir-Kheli, W. A. Goddard, *J. Phys. Chem. Lett.* **2011**, *2*, 212 – 217.

